Effect of magnetic frustration on nematicity and superconductivity in Fe chalcogenides

J. K. Glasbrenner,[1*] I. I. Mazin,[2] Harald O. Jeschke,[3] P. J. Hirschfeld,[4] and Roser Valentí[3]
[1] *National Research Council/Code 6393, Naval Research Laboratory, Washington, DC 20375, USA*
[2] *Code 6393, Naval Research Laboratory, Washington, DC 20375, USA*
[3] *Institut für Theoretische Physik, Goethe-Universität Frankfurt, 60438 Frankfurt am Main, Germany*
[4] *University of Florida, Gainsville, FL, USA and*
[*] *e-mail: james.glasbrenner.ctr@nrl.navy.mil*
(Dated: September 8, 2015)

Over the past few years Fe chalcogenides (FeSe/Te) have advanced to the forefront of Fe-based superconductors (FeBS) research. The most intriguing results thus far are for intercalated and monolayer FeSe, however experimental studies are still inconclusive. Yet, bulk FeSe itself remains an unusual case when compared with pnictogen-based FeBS, and may hold clues to understanding the more exotic FeSe-derivatives. The FeSe phase diagram is unlike the pnictides: the orthorhombic distortion, which is likely to be of a "spin-nematic" nature in numerous pnictides, is not accompanied by magnetic order in FeSe, and the superconducting transition temperature T_c rises significantly with pressure before decreasing. In this paper we show that the magnetic interactions in chalcogenides, as opposed to pnictides, demonstrate unusual (and unanticipated) frustration, which suppresses magnetic, but not nematic order, favors ferro-orbital order in the nematic phase and can naturally explain the nonmonotonic pressure dependence of the superconducting critical temperature $T_c(P)$.

While full consensus regarding the mechanism of high-temperature superconductivity in Fe-based superconductors (FeBS) remains elusive, nearly all researchers agree that it is unconventional and that it has a magnetic origin[1,2]. However, there is a divergence of opinions on the nature of the electrons responsible for magnetism. There is an itinerant approach based on calculating the spin susceptibility with moderate Coulomb (Hubbard) and Hund's interactions[3–10] as well as a localized approach where itinerant electrons responsible for conduction and the Fermi surface interact with local spins[11,12]. Finally, there is an increasingly popular description where the electrons have a dual character and provide the local moments, the interaction between them, and the electronic conductivity[13–16]. Within this picture, FeBS can still be reasonably mapped onto a short-range model of pairwise interactions between the local moments.

Following the discovery of the FeBS, there were multiple attempts to map the exchange interactions onto the Heisenberg model. The J_1-J_2 model on the square lattice[17] with nearest- (J_1) and next-nearest-neighbor (J_2) exchange couplings was a natural starting point[18–21], but required dramatically different couplings for ferro- and antiferromagnetic neighbors, $J_{1a} \ll J_{1b}$ to reproduce the observed spin waves[22,23] and *ab-initio* calculations[24]; it also failed to describe the double-stripe configuration in FeTe[25,26]. The model was extended to include third-neighbor exchange J_3[27] to reproduce the FeTe magnetic ground state. However, only the Ising model has this configuration as a solution, and in the Heisenberg model it is not a ground state for any set of parameters[28,29]. Therefore adding J_3 does not solve the problem. Besides, the $J_{1a} \ll J_{1b}$ implies an unphysical temperature dependence of the exchange constants (as T approaches T_N, by symmetry $J_{1a} \to J_{1b}$).

There were attempts to overcome these problems by adding the nearest-neighbor biquadratic exchange interaction $K(\mathbf{S}_i \cdot \mathbf{S}_j)^2$ to the J_1-J_2[24,30,31] or J_1-J_2-J_3[32] Heisenberg model. The three-neighbor Heisenberg model with biquadratic term (denoted J_1-J_2-J_3-K model from now on) eliminates the need for the $J_{1a,1b}$ anisotropy of the nearest-neighbor exchange and, for sufficiently large K and J_3, has a ground state consistent with that of FeTe. The biquadratic coupling in this model is also essential to explain the splitting between the antiferromagnetic and orthorhombic phase transitions in the Fe pnictides[18,33,34].

Whereas the magnetism in Fe-pnictides is successfully explained by the J_1-J_2-J_3-K model, the Fe-chalcogenides remain problematic. Specifically, there are two important unresolved controversies regarding bulk FeSe; (i) it shows a structural transition at $T_s \sim 90$ K but, contrary to the Fe-pnictides, no magnetic order is observed below T_s. Instead, an extended nematic region is detected[35,36] and the system becomes superconducting at $T_c \sim 8$ K. (ii) The superconducting T_c first increases with pressure and then decreases, forming a dome[37]. This is in apparent contradiction with the expectation of a decreasing T_c with pressure when magnetism is absent.

In the present work we propose a solution to this mystery and generalize the results to the family of Fe-chalcogenides FeSe/Te. We show, using *ab-initio* density functional theory calculations and effective model considerations, that many properties of FeSe/Te are related to its unusual magnetic frustration, absent in the Fe-pnictides. We show that J_1-J_2-J_3-K is the minimal spin model that includes the relevant complexity of the magnetism in Fe-chalcogenides. We then identify a new range of parameters appropriate for FeSe/Te where a highly competitive novel "staggered dimer" phase[38] is stabilized (recently shown to be the ground state of FeSe in *ab-initio* calculations[39]).

Exchange model and phase diagram

We define the J_1-J_2-J_3-K model on the square lattice as

$$H = \sum_{\text{nn}} \left[J_1 \hat{\mathbf{m}}_i \cdot \hat{\mathbf{m}}_j + K \left(\hat{\mathbf{m}}_i \cdot \hat{\mathbf{m}}_j \right)^2 \right] \quad (1)$$
$$+ \sum_{\text{2nn}} J_2 \hat{\mathbf{m}}_i \cdot \hat{\mathbf{m}}_j + \sum_{\text{3nn}} J_3 \hat{\mathbf{m}}_i \cdot \hat{\mathbf{m}}_j$$

The first sum is taken over all nearest neighbor $\{i, j\}$ pairs of Fe spins, the second one over all next nearest neighbors, *etc.* $\hat{\mathbf{m}}$ is the unit vector in the spin direction, $|\hat{\mathbf{m}}_i| \equiv 1$. For $K = 0(\infty)$, this model reduces to the already solved Heisenberg[29] (Ising[38]) on the square lattice.

To begin, we review the phase diagrams for the standard J_1-J_2-J_3 Ising and Heisenberg models. In Fig. 2a we show the mean-field $T = 0$ Ising phase diagram which includes the staggered dimer and double stripe ground states (see Fig. 1 for pattern definition). While this phase diagram can explain the *ab-initio* magnetic states of FeSe and FeTe, note that the Ising model is inapplicable to low-anisotropy materials such as the pnictides and chalcogenides, and the Heisenberg model is more appropriate[24,30–32]. The mean-field phase diagram for the Heisenberg model at $T = 0$ is shown in Fig. 2b (quantum corrections introduce minor changes[29]). The double stripe phase has measure zero [it is a degenerate case of $\mathbf{q} = (Q, Q)$]. This means that *no Heisenberg model can explain the formation of a collinear double stripe state*.

The review of the Ising and Heisenberg phase diagrams elucidates the two theoretical problems that have been underemphasized in previous analyses of the magnetic interactions of the Fe-based superconductors, especially in the chalcogenides: (1) the Heisenberg model does not account for all relevant magnetically ordered states and, by implication, does not properly describe spin fluctuations, and (2) the single and double stripe magnetic states are not the only important ground state candidates for the chalcogenides; there is a third one, the staggered dimers, which is highly competitive, but has been routinely ignored. To address these problems the biquadratic term, K, needs to be quantitatively taken into account.

We solved the full J_1-J_2-J_3-K model (Equation (1)) for general K in the mean-field limit and found six possible ground states (see Supplementary Materials). Hu *et. al.*[32] attempted prevously to solve this model, but missed the staggered dimer phase[39] which, we argue, is the key to understanding FeSe. A representative example phase diagram with $K = 0.1$ is shown in Fig. 2c. For a small, but non-zero K and J_3 the staggered dimer phase becomes stable in a narrow ($|J_2 - J_1/2| < 2\sqrt{2KJ_3}$) interval near the critical value $J_1 = 2J_2$, and at sufficiently large J_3 ($J_3 > J_1^2/8K$) the collinear double stripe structure is stabilized. As K grows, these collinear regions also grow, and at $K > J_1/2$ the phase diagram becomes identical to the Ising phase diagram in Fig. 2a. Actual materials will be seen to lie in the intermediate region, $0 < K \lesssim J_1/2$.

First-principles calculations

We performed density functional theory (DFT) calculations to obtain parameters for Equation (1) and place FeSe and FeTe into the context of the J_1-J_2-J_3-K phase diagram. There is a caveat though: due to the itinerant character of magnetism in FeBS, mapping onto local moments models such as Equation (1) has limited accuracy. A fundamental assumption of the standard Heisenberg model is that the magnetic moments are rigid, and this is an excellent assumption for systems with highly localized electrons, such as the high-T_c cuprates, but relatively poor for itinerant electrons. Magnetic interactions in metals tend to have long range tails, non-pairwise interactions, and the moments may depend on the magnetic ordering pattern. A clear example of the failure of the Heisenberg-biquadratic models is that the double stripe (Fig. 1b) and plaquette (see Fig. 1p in the Supplementary Material) configurations are degenerate in any such model, but in DFT the double stripe is 8 meV/Fe lower in energy than the plaquette configuration[40]. Therefore, we cannot expect to derive a Heisenberg model, with or without the biquadratic K, that captures exactly the energetics of all possible magnetic configurations.

Despite these limitations, the J_1-J_2-J_3-K model is the simplest framework that accounts for all the magnetic ground states that DFT and experiment find in different FeBS, and arguably is also the most complex one that still allows for an analytic solution. Since we are interested in spin fluctuation-driven effects such as superconductivity and spin-nematicity, which are low-energy phenomena, we establish a set of criteria for our fits, with the main goal to select a consistent set of magnetic states and obtain parameters that reproduce the low-energy hierarchy obtained within DFT. The criteria are detailed in the Methods section, and the chosen magnetic structures are shown in Fig. 1 panels a through e.

We performed calculations for FeSe at three representative pressures of 0, 4, and 9 GPa, and for FeTe at ambient pressure, see the Methods and Supplementary Materials for details. In all cases we used experimental lattice and internal parameters in tetragonal structures, as discussed in Methods. We fitted to the five magnetic configurations reported in Fig. 3 and extracted the J_1, J_2, and J_3 parameters. The biquadratic term was extracted from noncollinear calculations as in Ref. 40. The resulting J_1-J_2-J_3-K model parameters are reported in Table I. Note that the error bars reflect the fit inaccuracy, and not the much smaller errors of the underlying DFT calculations.

First of all, we confirmed that the "staggered dimer" configuration[38] is 13 meV/Fe lower in energy than the single stripe configuration and is the true DFT ground state for FeSe[39] (see Fig. 3). The same phase is also the lowest in energy in FeTe, as long as one does not take into account the magnetoelastic coupling. The calculated energy difference between the double stripe and staggered dimer configurations in tetragonal FeTe is tiny, $\sim 1 - 2$ meV/Fe. However, upon full structural relaxation into a monoclinic structure the double stripe pattern gains more magnetoelastic energy than the staggered dimer one (which relaxes into an orthorhombic structure) and ends up lower by a few meV, with the crystallographic distortion in agreement with experiment[25,26].

Another important result is that while the main contenders for the ground state of FeTe are the double stripe ($\mathbf{q}_{\rm ds} = (\pi/2, \pi/2)$) and the staggered dimer ($\mathbf{q}_{\rm di} = (\pi, \pi/2)$) structures, with the staggered trimers ($\mathbf{q}_{\rm tri} = (\pi, \pi/3)$) a close third, in FeSe the double stripe structure is not competitive at all. In FeSe the lowest energy states are the staggered dimers, trimers, tetramers and single stripes, with $\mathbf{q}$, respectively, $(\pi, \pi/2)$, $(\pi, \pi/3)$, $(\pi, \pi/4)$, and ($\mathbf{q}_{\rm ss} = (\pi, 0)$). From this, one can conclude that while in experiment the long range order of FeSe is destroyed by spin fluctuations, the most relevant ones are those with the corresponding wave vectors as listed above, and, very likely, with any $\mathbf{q} = (\pi, Q)$ such that $0 \leq Q \leq \pi/2$.

Importantly, when FeSe is structurally optimized in any of the low energy magnetic structures, it admits an orthorhombic structure quantitatively consistent with the experiment, $(a-b)/(a+b) \sim 0.2\%$, while optimization without magnetism never breaks the tetragonal symmetry. Furthermore, upon applying pressure, the hierarchy of states changes and the single stripe state becomes the lowest in energy, as can be seen in Fig. 3, thus making fluctuations at $\mathbf{q}_{\rm ss} = (\pi, 0)$ the leading mode.

Discussion

As mentioned, there are two outstanding experimental paradoxes regarding FeSe. The first paradox concerns the splitting of the orthorhombic and magnetic transition observed in Fe pnictides, which is taken to an extreme in FeSe: the structural transition occurs at $T_s \sim 90$ K, but no magnetic order follows. Yet, exactly as in the pnictides, DFT calculations reproduce the distorted structure when the calculated ground state magnetic structure is used, but show no tendency towards orbital ordering or a structural distortion if magnetization is kept zero.

The second paradox deals with the behavior of the critical superconducting temperature with pressure $T_c(P)$. Typically, pressure has a tendency to suppress magnetism, so in the context of a magnetic pairing mechanism, pressure is beneficial to superconductivity when magnetic order is present, but it is destructive if it is not. For the nonmagnetic FeSe, the expectation then is that T_c should decrease monotonically with pressure. Instead, T_c first increases and then decreases with pressure, forming a characteristic dome shape[37]. In the following we discuss how the J_1-J_2-J_3-K model resolves these paradoxes.

First we analyze the J_1-J_2-J_3-K model parameters given in Table I and plotted in Fig. 2. The crosses in Figs 2d, 2e, and 2f, show the placement of FeSe at 9 GPa, FeSe at 0 GPa, and FeTe at 0 GPa, respectively, in the J_1-J_2-J_3-K phase diagram. Interestingly, for both FeSe and FeTe the calculated ground state at ambient pressure is near a phase boundary: between the staggered dimer phase and the single stripe phase for FeSe and between the staggered dimer phase and double stripe phase for FeTe. Note that FeTe appears to be very close to an Ising model because of the large K and not because of a large magnetic anisotropy.

Generally speaking, one can anticipate that, in the absence of long-range order, spin fluctuations with wave vectors corresponding to the lowest energy states will occur: Thus, in FeTe one expects fluctuations with $\mathbf{q}_{\rm ds}$, $\mathbf{q}_{\rm di}$, and $\mathbf{q}_{\rm tri}$. None of those would support $s_\pm$ superconductivity since only fluctuations with $\mathbf{q} \sim \mathbf{q}_{\rm ss}$ can pair electrons in the standard $s_\pm$ superconducting state. They all break tetragonal symmetry, but in different ways, incompatible with each other, and cannot all support the same nematic state. In FeSe, by contrast, one expects fluctuations with $\mathbf{q} = (\pi, Q)$, where $Q = 0$, $\pi/4$, $\pi/3$, and $\pi/2$ (while we cannot check this, likely all fluctuations with $\mathbf{q} = (\pi, Q)$, where $-\pi/2 \lesssim Q \lesssim \pi/2$ are supported, cf. Fig. 4 **a**). This is very different from Fe pnictides, where the single stripe state is much lower in energy than all other patterns, and therefore the $\mathbf{q}_{\rm ss}$ fluctuations dominate. Note that the above results rely upon the fact that Fe in FeBS has a large *local* moment (even larger than in DFT),[41] and cannot be obtained by linear response calculations based on a paramagnetic phase[42].

The most important consequence of our findings is that different spin fluctuations in FeSe (but not FeTe), while mutually incompatible with regards to long range magnetic order, break tetragonal symmetry in the same way (and the same is true for all $\mathbf{q} = (\pi, Q)$, $-\pi/2 \lesssim Q \lesssim \pi/2$). In other words, one can have a suppression of long-range magnetic ordering due to the competing fluctuations with $\mathbf{q} = (\pi, Q)$ for different Qs, but at the same time these fluctuations all break the $x \leftrightarrow y$ symmetry and do not compete in terms of nematicity. Note that the double-stripe fluctuations with $\mathbf{q}_{\rm ds} = (\pi/2, \pi/2)$ break a different symmetry, $x+y \leftrightarrow x-y$, and thus do compete nematically with the single-stripe ones in FeTe. Therefore FeSe represents a special case where several different types of spin fluctuations are simultaneously excited, which prevents them from condensing at any one wave vector and forming long range magnetic order, but does not prevent the formation of the nematic orthorhombic order. We emphasize that this nematic order, just as the underlying incipient magnetic one, is accompanied by considerable orbital ordering. We find (see Fig. 4 **c**) that all investigated $\mathbf{q} = (\pi, Q)$ states induce population imbalance between the Fe(d_{xz}) and Fe(d_{yz}) orbitals on each Fe site of the order of $(n_{xz} - n_{yz})/(n_{xz} + n_{yz}) \approx 8\%$. This observation proves that the orbital ordering is *not* sensitive to the magnetic long range order, but only to the nematic order, and has multiple ramifications. The orbital ordering can be probed experimentally, and was observed in the nematic phase at $T \lesssim T_s$ by the Knight shift anisotropy[35], while a divergence in $1/TT_1$, as expected, was only observed at much lower temperatures, upon approaching the long range magnetic order at $T \sim 0$.

Let us now address the intriguing pressure dependence of T_c. In general, pressure reduces magnetic interactions in FeSe. However, the staggered dimer state is suppressed with pressure faster than the single stripe state (Fig. 3), so that instead of multiple competing types of fluctuation we obtain a situation similar to the pnictides, where fluctuations with $\mathbf{q} = (\pi, 0)$ decisively dominate. Note that in the $s_\pm$ model these are the fluctuations that are responsible for superconductivity. At ambient pressure, the staggered dimer/trimer fluctuations are dominant, but cannot lead to pairing, since

the very small FeSe Fermi pockets are not connected by $\mathbf{q} = (\pi, Q)$, where $Q \sim \pi/2$. As discussed in Ref. 43, such low energy fluctuations with "wrong" momenta are pairbreaking since they act essentially as impurities (note that the situation in FeSe is qualitatively different from previous discussions in which fluctuations in different channels compete[44], but can in principle each lead to pairing).

Under pressure the pairbreaking staggered dimer and trimer spin fluctuations are seen to decrease in amplitude much more rapidly than the pairing stripe spin fluctuations at $\mathbf{q} = (\pi, 0)$. This removal of pairbreaking effects is responsible for the initial increase in T_c. The further increase of pressure decreases the amplitude of *both* the pairbreaking $\mathbf{q} = (\pi, Q)$ and pairing $\mathbf{q} = (\pi, 0)$ fluctuations, leading to the dome-like behavior of T_c vs. pressure.

Even more importantly, the nematic order, which is strongest at $P = 0$, gradually weakens with pressure, as the $\mathbf{q} = (\pi, Q)$ ($Q \sim \pi/2$) fluctuations are suppressed. As shown in Fig. 4 **b**, the density of states at the Fermi level $N(0)$ is strongly decreased in all nematic-compatible states compared to the paramagnetic or Néel states, which is detrimental for superconductivity (and vice-versa, as observed in $BaFe_{2-x}Co_xAs_2$[45]). This result indicates that long-range orbital, not magnetic, ordering leads to a sharp reduction in the Fermi surface and thereby $N(0)$, which is consistent with photoemission and quantum oscillation experiments[46,47]. Since T_c is exponentially dependent on N(0), the suppression of nematicity with pressure is another factor ensuring the initial rise of T_c.

Conclusions

We presented a detailed analysis, based on first principles calculations, of magnetic interactions in the FeSe/Te family. We show that in FeSe the magnetic interactions are much more frustrated than in either FeTe or the Fe pnictides. We argue that the simultaneous excitation of spin fluctuations with various wave vectors of the type $\mathbf{q} = (\pi, Q)$ prevent long-range magnetic ordering in FeSe, but does allow for the usual spin-nematic order accompanied by a ferro-orbital order. At zero pressure the leading fluctuations are nonpairing (in the $s_\pm$ channel) $Q = \pi/2$ ones, but pairing fluctuations at $Q = 0$ become the leading fluctuations with pressure, which explains the unusual nonmonotonic pressure dependence of T_c.

To be able to analyze the emerging situation on a model level, we mapped the low-energy energetics onto a three neighbors Heisenberg + biquadratic exchange Hamiltonian, which we have solved analytically at $T = 0$ in the mean field approximation. It appears that the biquadratic interaction is essential to stabilize the observed double stripe phase in FeTe; without the extra term, this phase can never be the ground state at any choice of parameters. The same is true for the staggered dimer phase found to be the DFT ground state in FeSe. A nontrivial combination of the biquadratic and third-neighbor exchanges, in addition to the usually considered first and second neighbor Heisenberg interactions, ensures the anomalously large splitting of the nematic and antiferromagnetic transitions (in FeSe, it leads to a total suppression of magnetic ordering). We believe that this new perspective on the unusual magnetic physics of Fe chalcogenides will be crucial to an explanation of their remarkable properties, including perhaps high temperature superconductivity in the monolayer FeSe system.

Methods

We employed density functional theory and made use of three separate, full potential (all electron) codes, ELK, WIEN2K, and FPLO to calculate the energies. The generalized gradient approximation was used for the exchange-correlation functional. We checked for convergence with respect to k-points and, for ELK, the number of empty states. We calculated the energies of multiple collinear configurations using all three codes for comparison purposes, while noncollinear calculations were handled exclusively by the ELK code. The comparison of all the different collinear configuration energies can be found in the Supplementary Materials.

We used the tetragonal P4/nmm space group (origin choice 2) for the crystal structure of FeSe and FeTe in all our calculations. The Fe and chalcogenide (Se/Te) ions occupy the 2a and 2c Wyckoff positions, respectively. The lattice parameters for the different materials (and for FeSe, under different pressures) are summarized in Table II. We note that at low temperatures FeSe is strictly an orthorhombic structure, but this distortion is small and omitting it leads to a small magnetoelastic error when compared with the exchange parameter energy scales. Furthermore, we are interested in the physics that emerges from spin fluctuations that originate in the tetragonal phase. Therefore, for FeSe, we defined a volume-conserving effective parameter $a^* = \sqrt{ab}$, where a and b are the orthorhombic parameters taken from experiment.

We fit to the Hamiltonian in Equation (1) in the usual way. The details of how the fit was performed are given in the Supplementary Materials. It was not possible to achieve a fit that accurately reproduced all energies for all possible collinear configurations, so we defined a set of criteria for our fitting procedure. The criteria were (1) collinear ground states of the J_1-J_2-J_3-K model should be included, (2) low energy structures that do not suffer from moment collapse under pressure (for FeSe) should be included, (3) local moments of included structures should be similar, and (4) we exclude configurations that yield fits that do not reproduce the density functional theory energy hierarchy of the lowest energy configurations. The fourth criterion is necessary because we cannot produce an accurate fit for all configurations, so we decide which features of the density functional theory set of energies is important from the point of view of fluctuations and frustration, which are the lowest energy ones. Given these criteria, we perform the fitting procedure using the energies summarized in Fig. 3.

Acknowledgments

We thank M. Tomić for running some test calculations at the initial stages of this work and D. Guterding, S. Backes, A. Coldea, R. Fernandes, N. Perkins, S. Kivelson and Wei Ku for valuable discussions. I.I.M. is supported by ONR through the NRL basic research program. J.K.G. acknowl-

edges the support of the NRC program at NRL. H.O.J. and R.V. are supported by DFG-SPP1458. P.J.H. was partially supported by US DOE DE-FG02-05ER46236.

Author contributions

I.I.M. and J.K.G. conceived the research; J.K.G., I.I.M. and H.O.J. carried out numerical calculations; all authors participated in the discussion and contributed to writing the paper; I.I.M. and R.V. supervised the whole project.

SUPPLEMENTARY MATERIAL

Supplementary Methods

We calculated the energy of a variety of different collinear structures using the three different codes, ELK[48], WIEN2K[49], and FPLO[50]. The generalized gradient approximation was used for the exchange-correlation functional[51]. The structures in Fig. 5 summarize all of the different configurations that we considered. In Fig. 6 are the energies we calculated using these codes. Note that we did not calculate the energy of every configuration using all three codes, but there are several points of comparison. For all configurations for which we can make a comparison, there is excellent agreement across codes. The most important result of this comparison is that there is no ambiguity as to the energy hierarchy of the low-lying energy states, it is the same for all three codes. We also note that the energy range for the different configurations is quite large for both FeSe and FeTe, on the scale of $100-300$ meV for FeSe and $50-100$ meV for FeTe.

We fitted to the Heisenberg model with the ordinary least squares (OLS) method using the Heisenberg model coefficients reported in Table III for our collinear fits and the expression $\Delta E(\theta) = E(\theta) - E(0) = 2K\sin^2(\theta)$, see Ref.[40] for the definition of θ, for our noncollinear fits. The noncollinear energies and the corresponding fits are shown in Fig. 7.

As reported in the main article, the collinear fits are very good for the included configurations, but there are deviations if we apply the model to configurations excluded due to the criteria we outlined in the main Methods section. This is a consequence of the itinerant nature of the magnetism, which in general cannot be mapped onto a pairwise interaction model. We also note that the lower symmetry magnetic structures, such as those with generic names such as "dduuduuu," suffered moment collapse in FeSe under pressure. The noncollinear fits, on the other hand, are excellent.

It is worth noting that for itinerant magnets the exchange model could be potentially improved using an approach similar to Moriya[52] and allowing the moment amplitudes to vary and by also including Stoner-like onsite terms. We tried including terms like this to see how it affected the quality of our fits. We found that including these terms does not change the fitting results in any qualitative way when using the configurations in Table III. Furthermore, it did not allow us to extend the fit to also reproduce the high-energy configurations from Fig. 5. It is possible, however, that these modifications would be important for fluctuations above the Néel temperature.

Phase boundaries of J_1-J_2-J_3-K model

Here we give additional details of the analytic solution of the J_1-J_2-J_3-K model. First, let us ignore the K term and refresh what is known about the $J_1-J_2-J_3$ Heisenberg models. The Ising model has four phases, the checkerboard (cb) phase in Fig. 5a, the double stripe (ds) phase in Fig. 5d, the single stripe (ss) phase in Fig. 5e, and the staggered dimers (di) phase in Fig. 5f. The Heisenberg model also has four phases, but neither the ds or di phase are ground states in the phase diagram. Instead, the four phases are the aforementioned cb and ss phases, and in addition two spiral phases with spins rotating away from the origin as $\alpha = n_x q_x + n_y q_y$, the first with wavevector $\mathbf{q}_1 = (\pi, Q)$ and the second with $\mathbf{q}_2 = (Q, Q)$ (see, e.g., Ref.[53]). Note that at $\mathbf{q}_1(Q \to 0) = (\pi, 0)$, which is the ss phase, and at $\mathbf{q}_1(Q \to \pi) = \mathbf{q}_2(Q \to \pi) = (\pi, \pi)$, which is the cb phase. In both phases Q depends on the exchange parameters: $Q = \cos^{-1}\left[(2J_2 - J_1)/4J_3\right]$ for $\mathbf{q}_1$ and $Q = \pi - \cos^{-1}\left[J_1/(2J_2 + 4J_3)\right]$ for $\mathbf{q}_2$. Finally, the analytic expressions for the phase boundaries are summarized in Table IV.

Adding in the biquadratic term $-K\left(\hat{\mathbf{m}}_i \cdot \hat{\mathbf{m}}_j\right)^2$ restores the ds and di configurations to the phase diagram. The allowed wavevectors in the spin spiral phases also become dependent on K: $Q = \cos^{-1}\left[(2J_2 - J_1)/(4J_3 - 2K)\right]$ for $\mathbf{q}_1$ and $Q = \pi - \cos^{-1}\left[J_1/(2J_2 + 4J_3 - 2K)\right]$ for $\mathbf{q}_2$. The analytic expressions for the phase boundaries also change and many become K-dependent as summarized in the last column of Table IV. As K grows so do the areas of stability of the ds and di phases. Once $K > J_1/2$, the phase diagram becomes indistinguishable from the Ising model.

$FeSe_{0.5}Te_{0.5}$

A notable omission to our results is the case of $FeSe_{0.50}Te_{0.50}$. Unlike the other materials, the structure of $FeSe_{0.50}Te_{0.50}$ is not well-defined. A common approach is to use lattice parameters from experiment and then choose the chalcogenide to be either pure Se or pure Te, assuming that the change in the lattice parameters drives the relevant physics, such as inducing superconductivity. A check of this reveals that this is not entirely the case; there is a significant energy splitting of the checkerboard, double stripe, and zig-zag configurations when Se/Te are swapped, and the energy splits are not in the same direction. Using Te lowers the checkerboard energy, while it increases the double stripe energy, for example. Furthermore, careful experimental analysis reveals that $FeSe_{0.50}Te_{0.50}$ is a disordered structure with different heights for Se and Te[54]. Taking this into account requires an expensive and non-trivial averaging procedure. While a description of $FeSe_{0.50}Te_{0.50}$ would be useful, we put the question aside for now due to the complexity of the structure.

[1] Chubukov, A. Pairing Mechanism in Fe-Based Superconductors. *Annu. Rev. Condens. Matter Phys.* **3**, 57 (2012).

[2] Hirschfeld, P. J., Korshunov, M. M. & Mazin, I. I. Gap symmetry and structure of Fe-based superconductors. *Rep. Prog. Phys.* **74**, 124508 (2011).

[3] Wang, F., Zhai, H. & Lee, D.-H. Antiferromagnetic correlation and the pairing mechanism of the cuprates and iron pnictides: A view from the functional renormalization group studies. *Europhys. Lett.* **85**, 37005 (2009).

[4] Chubukov, A. V., Efremov, D. V. & Eremin, I. Magnetism, superconductivity, and pairing symmetry in iron-based superconductors. *Phys. Rev. B* **78**, 134512 (2008).

[5] Stanev, V., Kang, J. & Tesanovic, Z. Spin fluctuation dynamics and multiband superconductivity in iron pnictides. *Phys. Rev. B* **78**, 184509 (2008).

[6] Kuroki, K. *et al.* Unconventional Pairing Originating from the Disconnected Fermi Surfaces of Superconducting $LaFeAsO_{1-x}F_x$. *Phys. Rev. Lett.* **101**, 087004 (2008).

[7] Graser, S., Maier, T. A., Hirschfeld, P. J. & Scalapino, D. J. Near-degeneracy of several pairing channels in multiorbital models for the Fe pnictides. *New J. Phys.* **11**, 025016 (2009).

[8] Sknepnek, R., Samolyuk, G., Lee, Y.-B. & Schmalian, J. Anisotropy of the pairing gap of FeAs-based superconductors induced by spin fluctuations. *Phys. Rev. B* **79**, 054511 (2009).

[9] Yao, Z.-J., Li, J.-X. & Wang, Z. D. Spin fluctuations, interband coupling and unconventional pairing in iron-based superconductors. *New J. Phys.* **11**, 025009 (2009).

[10] Guterding, D., Jeschke, H. O., Hirschfeld, P. J. & Valentí, R. Unified picture of the doping dependence of superconducting transition temperatures in alkali metal/ammonia intercalated FeSe. *Phys. Rev. B* **91**, 041112 (2015).

[11] Seo, K., Bernevig, B. A. & Hu, J. Pairing Symmetry in a Two-Orbital Exchange Coupling Model of Oxypnictides. *Phys. Rev. Lett.* **101**, 206404 (2008).

[12] Lv, W., Krüger, F. & Phillips, P. Orbital ordering and unfrustrated $(\pi, 0)$ magnetism from degenerate double exchange in the iron pnictides. *Phys. Rev. B* **82**, 045125 (2010).

[13] Dai, P., Hu, J. & Dagotto, E. Magnetism and its microscopic origin in iron-based high-temperature superconductors. *Nat. Phys.* **8**, 709 (2012).

[14] Moon, S. J. *et al.* Dual character of magnetism in $EuFe_2As_2$: Optical spectroscopic and density-functional calculation study. *Phys. Rev. B* **81**, 205114 (2010).

[15] Lee, H., Zhang, Y.-Z., Jeschke, H. O. & Valentí, R. Possible origin of the reduced ordered magnetic moment in iron pnictides: A dynamical mean-field theory study. *Phys. Rev. B* **81**, 220506 (2010).

[16] Yin, Z. P., Haule, K. & Kotliar, G. Kinetic frustration and the nature of the magnetic and paramagnetic states in iron pnictides and iron chalcogenides. *Nat. Mater.* **10**, 932 (2011).

[17] Chandra, P., Coleman, P. & Larkin, A. I. Ising transition in frustrated Heisenberg models. *Phys. Rev. Lett.* **64**, 88 (1990).

[18] Xu, C., Müller, M. & Sachdev, S. Ising and spin orders in the iron-based superconductors. *Phys. Rev. B* **78**, 020501 (2008).

[19] Fang, C., Yao, H., Tsai, W.-F., Hu, J. & Kivelson, S. A. Theory of electron nematic order in LaFeAsO. *Phys. Rev. B* **77**, 224509 (2008).

[20] Ma, F., Lu, Z.-Y. & Xiang, T. Arsenic-bridged antiferromagnetic superexchange interactions in LaFeAsO. *Phys. Rev. B* **78**, 224517 (2008).

[21] Si, Q. & Abrahams, E. Strong Correlations and Magnetic Frustration in the High T_c Iron Pnictides. *Phys. Rev. Lett.* **101**, 076401 (2008).

[22] Zhao, J. *et al.* Spin waves and magnetic exchange interactions in $CaFe_2As_2$. *Nat. Phys.* **5**, 555 (2009).

[23] Diallo, S. O. *et al.* Itinerant Magnetic Excitations in Antiferromagnetic $CaFe_2As_2$. *Phys. Rev. Lett.* **102**, 187206 (2009).

[24] Yaresko, A. N., Liu, G.-Q., Antonov, V. N. & Andersen, O. K. Interplay between magnetic properties and Fermi surface nesting in iron pnictides. *Phys. Rev. B* **79**, 144421 (2009).

[25] Li, S. *et al.* First-order magnetic and structural phase transitions in $Fe_{1+y}Se_xTe_{1+x}$. *Phys. Rev. B* **79**, 054503 (2009).

[26] Bao, W. *et al.* Tunable $(\delta\pi, \delta\pi)$-Type Antiferromagnetic Order in α-Fe(Te,Se) Superconductors. *Phys. Rev. Lett.* **102**, 247001 (2009).

[27] Ma, F., Ji, W., Hu, J., Lu, Z.-Y. & Xiang, T. First-Principles Calculations of the Electronic Structure of Tetragonal α-FeTe and α-FeSe Crystals: Evidence for a Bicollinear Antiferromagnetic Order. *Phys. Rev. Lett.* **102**, 177003 (2009).

[28] Ferrer, J. Spin-liquid phase for the frustrated quantum Heisenberg antiferromagnet on a square lattice. *Phys. Rev. B* **47**, 8769 (1993).

[29] Sindzingre, P., Shannon, N. & Momoi, T. Phase diagram of the spin-1/2 $J_1 - J_2 - J_3$ Heisenberg model on the square lattice. *J. Phys. Conf. Ser.* **200**, 022058 (2010).

[30] Wysocki, A. L., Belashchenko, K. D. & Antropov, V. P. Consistent model of magnetism in ferropnictides. *Nat. Phys.* **7**, 485 (2011).

[31] Wysocki, A. L., Belashchenko, K. D., Ke, L., van Schilfgaarde, M. & Antropov, V. P. Biquadratic magnetic interaction in parent ferropnictides. *J. Phys. Conf. Ser.* **449**, 012024 (2013).

[32] Hu, J., Xu, B., Liu, W., Hao, N.-N. & Wang, Y. Unified minimum effective model of magnetic properties of iron-based superconductors. *Phys. Rev. B* **85**, 144403 (2012).

[33] Fernandes, R. M., Chubukov, A. V., Knolle, J., Eremin, I. & Schmalian, J. Preemptive nematic order, pseudogap, and orbital order in the iron pnictides. *Phys. Rev. B* **85**, 024534 (2012).

[34] Mazin, I. I. & Schmalian, J. Pairing symmetry and pairing state in ferropnictides: Theoretical overview. *Physica C* **469**, 614 (2009).

[35] Baek, S.-H. *et al.* Orbital-driven nematicity in FeSe. *Nat. Mater.* (2014).

[36] Böhmer, A. E. *et al.* Origin of the Tetragonal-to-Orthorhombic Phase Transition in FeSe: A Combined Thermodynamic and NMR Study of Nematicity. *Phys. Rev. Lett.* **114**, 027001 (2015).

[37] Medvedev, S. *et al.* Electronic and magnetic phase diagram of β-$Fe_{1.01}Se$ with superconductivity at 36.7 K under pressure. *Nat. Mater.* **8**, 630 (2009).

[38] Landau, D. P. & Binder, K. Phase diagrams and critical behavior of Ising square lattices with nearest-, next-nearest-, and third-nearest-neighbor couplings. *Phys. Rev. B* **31**, 5946 (1985).

[39] Cao, H.-Y., Chen, S., Xiang, H. & Gong, X.-G. Antiferromagnetic ground state with pair-checkboard order in FeSe. Preprint at <http://arxiv.org/abs/1407.7145>.

[40] Glasbrenner, J. K., Velev, J. P. & Mazin, I. I. First-principles study of the minimal model of magnetic interactions in Fe-based superconductors. *Phys. Rev. B* **89**, 064509 (2014).

[41] Mannella, N. The magnetic moment enigma in Fe-based high

temperature superconductors. *J. Phys. Condens. Mat.* **26**, 473202 (2014).

[42] Yin, Z. P., Haule, K. & Kotliar, G. Spin dynamics and orbital-antiphase pairing symmetry in iron-based superconductors. *Nat. Phys.* **10**, 845 (2014).

[43] Millis, A. J., Sachdev, S. & Varma, C. M. Inelastic scattering and pair breaking in anisotropic and isotropic superconductors. *Phys. Rev. B* **37**, 4975 (1988).

[44] Fernandes, R. M. & Millis, A. J. Nematicity as a Probe of Superconducting Pairing in Iron-Based Superconductors. *Phys. Rev. Lett.* **111**, 127001 (2013).

[45] Nandi, S. *et al.* Anomalous Suppression of the Orthorhombic Lattice Distortion in Superconducting $Ba(Fe_{1-x}Co_x)_2As_2$ Single Crystals. *Phys. Rev. Lett.* **104**, 057006 (2010).

[46] Terashima, T. *et al.* Anomalous Fermi surface in FeSe seen by Shubnikov-de Haas oscillation measurements. *Phys. Rev. B* **90**, 144517 (2014).

[47] Coldea, A. Private communication.

[48] ELK FP-LAPW Code [http://elk.sourceforge.net/].

[49] Blaha, P., Schwarz, K., Madsen, G. K. H., Kvasnicka, D. & Luitz, J. *WIEN2k, An Augmented Plane Wave + Local Orbitals Program for Calculating Crystal Properties* (Techn. Universität Wien, Austria, 2001).

[50] Koepernik, K. & Eschrig, H. Full-potential nonorthogonal local-orbital minimum-basis band-structure scheme. *Phys. Rev. B* **59**, 1743 (1999).

[51] Perdew, J. P., Burke, K. & Ernzerhof, M. Generalized Gradient Approximation Made Simple. *Phys. Rev. Lett.* **77**, 3865 (1996).

[52] Moriya, T. *Spin Fluctuations in Itinerant Electron Magnetism* (Springer, Berlin, 1985).

[53] Pimpinelli, A. & Rastelli, E. Absence of long-range order in three-dimensional spherical models. *Phys. Rev. B* **42**, 984 (1990).

[54] Louca, D. *et al.* Local atomic structure of superconducting $FeSe_{1-x}Te_x$. *Phys. Rev. B* **81**, 134524 (2010).

[55] Margadonna, S. *et al.* Pressure evolution of the low-temperature crystal structure and bonding of the superconductor FeSe ($T_c = 37$ K). *Phys. Rev. B* **80**, 064506 (2009).

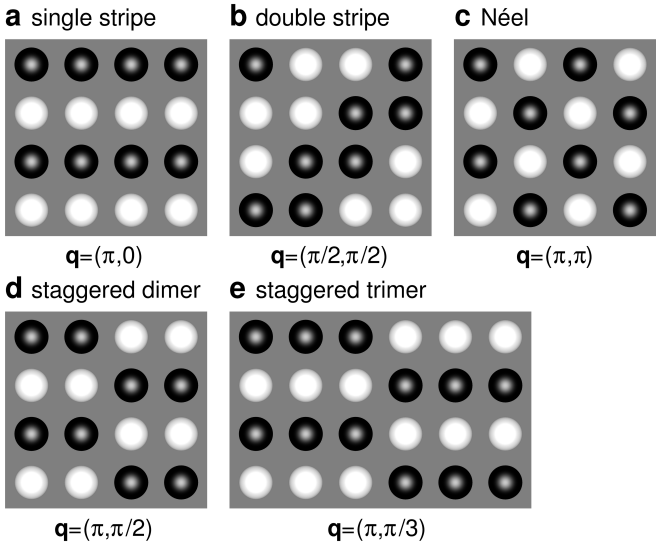

FIG. 1. **Collinear magnetic structures used for fitting to the J_1-J_2-J_3-K model.** (a) single stripe, (b) double stripe, (c) checkerboard (Néel), (d) staggered dimer, and (e) staggered trimer state.

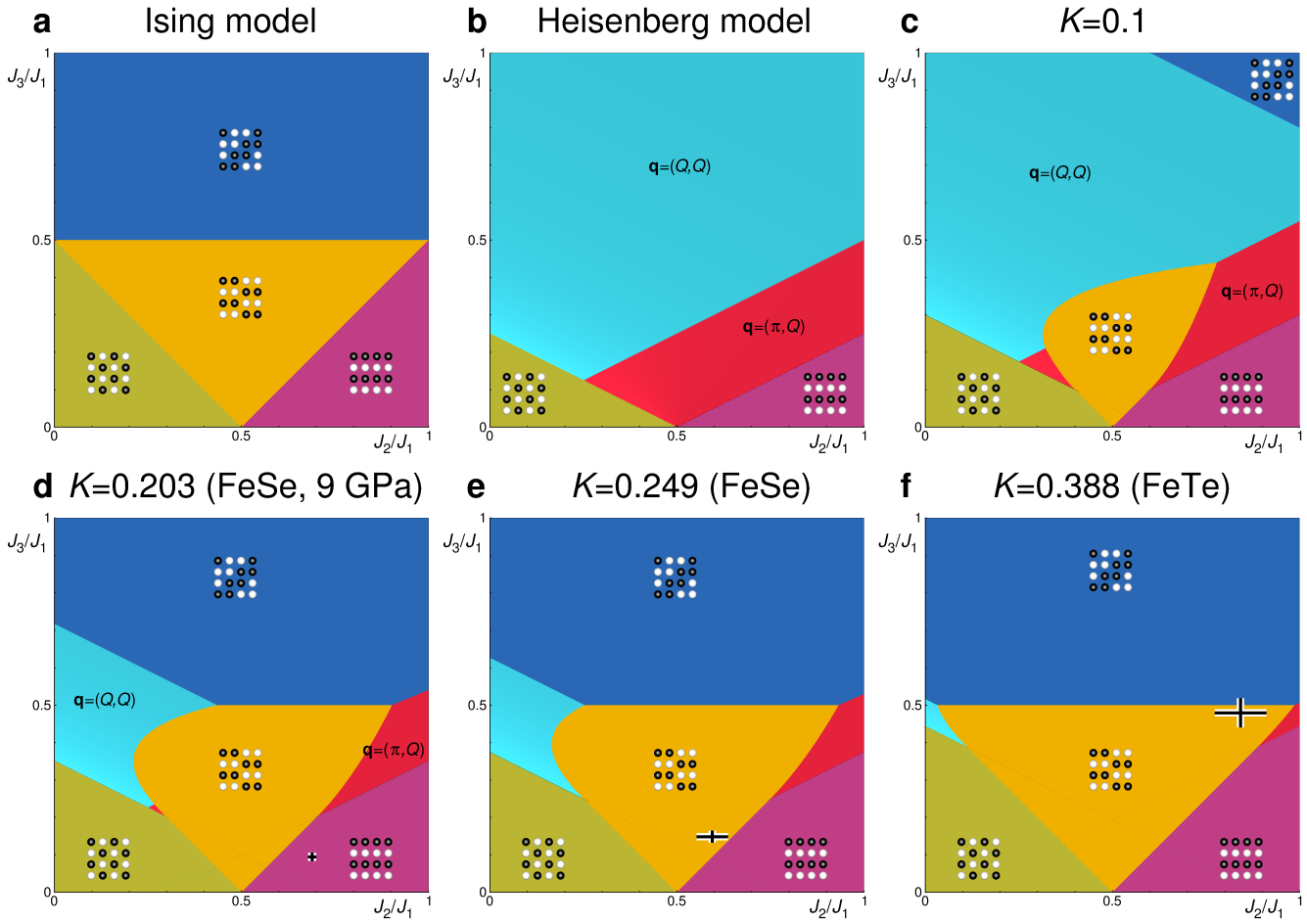

FIG. 2. **Classical mean-field phase diagrams.** **a**, The J_1-J_2-J_3 Ising model. **b**, The J_1-J_2-J_3 Heisenberg model. **c**, The J_1-J_2-J_3-K model with $K = 0.1$. **d**, The J_1-J_2-J_3-K model with $K = 0.20$ where the cross corresponds to FeSe at 9 GPa of pressure. **e**, The J_1-J_2-J_3-K model with $K = 0.25$ where the cross corresponds to FeSe at 0 GPa of pressure. **f**, The J_1-J_2-J_3-K model with $K = 0.39$ where the cross corresponds to FeTe at 0 GPa of pressure. The length of the cross' bars in panels **d** through **f** indicate the uncertainty of the fit to the J_1-J_2-J_3-K model.

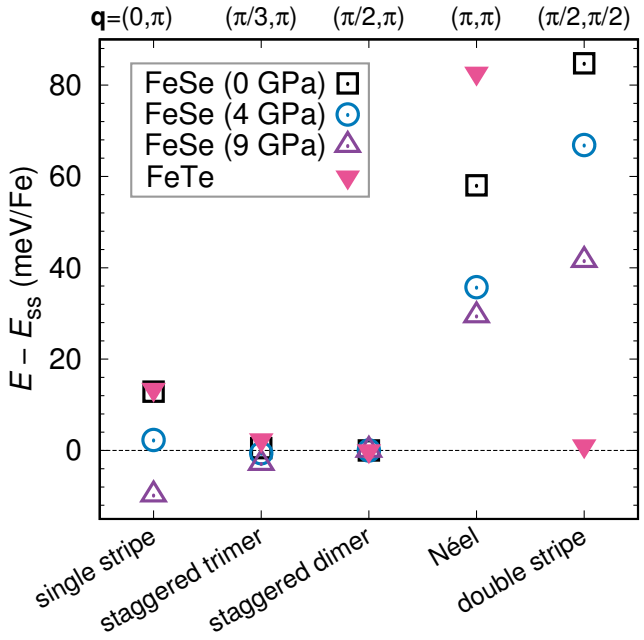

FIG. 3. **Energies of collinear magnetic configurations.** The total calculated DFT energies of the collinear magnetic configurations used in the fits of the J_1-J_2-J_3-K model.

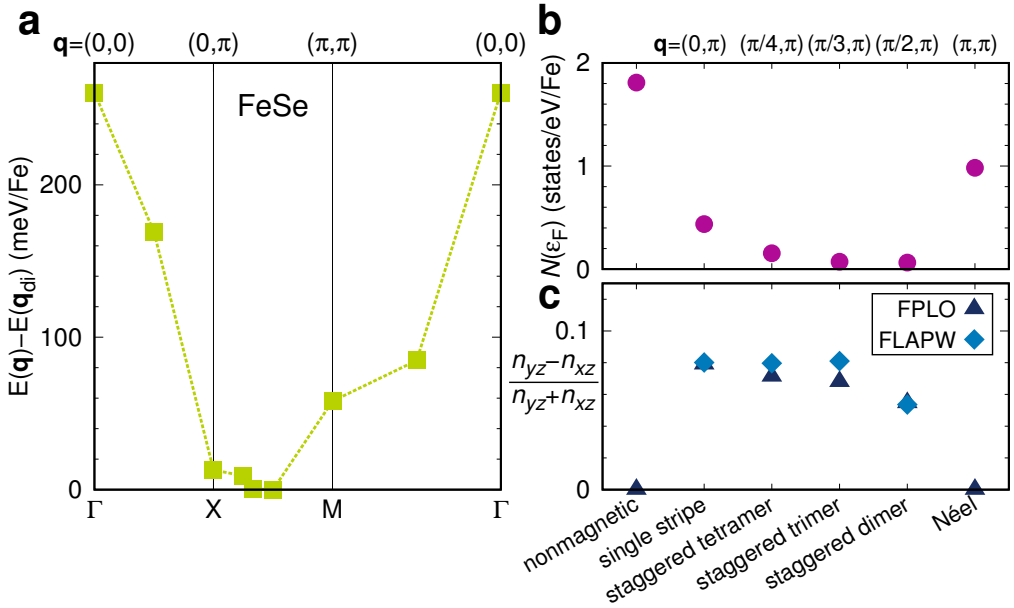

FIG. 4. **Energies, density of states at ε_F and orbital order of FeSe at 0 GPa pressure. a** The energies of collinear magnetic configurations of FeSe at ambient pressure plotted as a function of **q**. **b** $N(\varepsilon_F)$ for the lowest energy magnetic configurations compared to the nonmagnetic states indicates very small Fermi surfaces in fluctuating magnetic states. **c** Ferro-orbital order in Fe $3d_{xz}/d_{yz}$ orbitals measured for several magnetic states.

Material	J_1	J_2	J_3	K
		(meV)		
FeSe (0 GPa)	123.1 ± 6.5	73.0 ± 3.3	18.3 ± 1.8	30.6 ± 0.4
FeSe (4 GPa)	86.9 ± 2.4	51.9 ± 1.2	9.7 ± 0.6	15.7 ± 0.2
FeSe (9 GPa)	51.1 ± 0.7	35.4 ± 0.3	4.9 ± 0.2	10.4 ± 0.1
FeTe	50.7 ± 3.6	42.8 ± 1.8	24.4 ± 1.0	19.7 ± 0.2

TABLE I. **Heisenberg and biquadratic exchange parameters for FeSe/Te.** The parameters for FeSe are reported at three different pressures, 0 GPa, 4 GPa, and 9 GPa. FeTe is reported at 0 GPa. The reported uncertainties indicate the inaccuracy of the fit to the J_1-J_2-J_3-K model.

Material	a (Å)	c (Å)	z_{Se}	z_{Te}
FeSe	3.76976	5.52122	0.2688	
FeTe	3.81362	6.25381		0.2829
FeSe (4 GPa)	3.6717	5.1943	0.2740	
FeSe (9 GPa)	3.6049	5.0304	0.2839	

TABLE II. **Crystal parameters for FeSe and FeTe.** The structure parameters and Wyckoff positions for FeSe/Te, with FeSe reported at three different pressures. The 4 and 9 GPa parameters are from Ref. 55, where we defined an effective tetragonal lattice parameter $a^* = \sqrt{ab}$ using the inplane orthorhombic lattice parameters a and b.

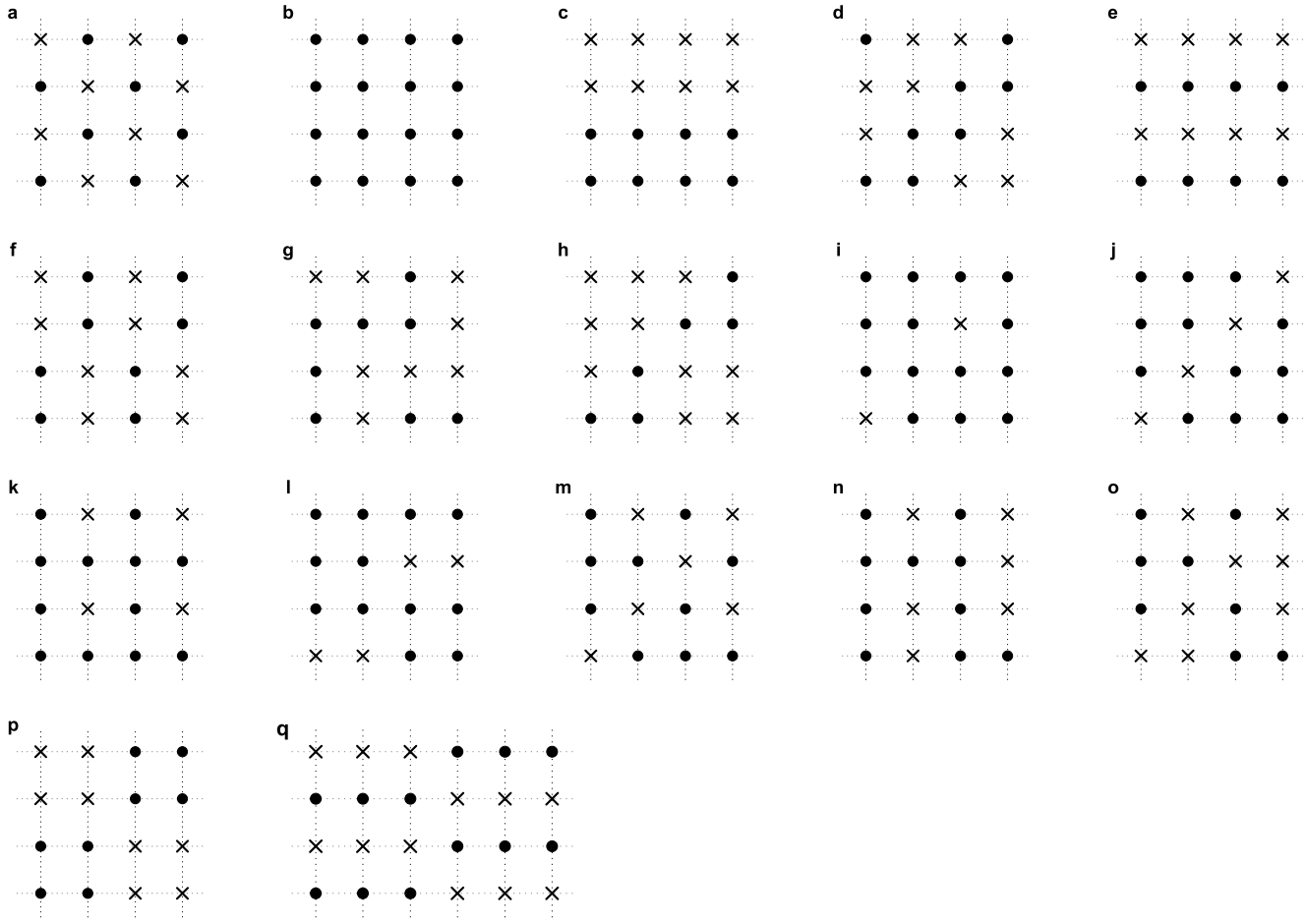

FIG. 5. **Collinear magnetic structures a**, Checkerboard (cb). **b**, Ferromagnetic (fm). **c**, Parallel Stripes (parastr). **d**, Double Stripe (ds). **e**, Single Stripe (ss). **f**, Staggered Dimers (di). **g**, Zig-zag Stripes (zigzag). **h**, dduuduuu. **i**, duuuuuuu. **j**, dduuuuuu. **k**, uddduuuu. **l**, duuuduuu. **m**, ddduuuuu. **n**, uddduduu. **o**, ddduduuu. **p**, plaquette. **q**, Staggered Trimers (tri).

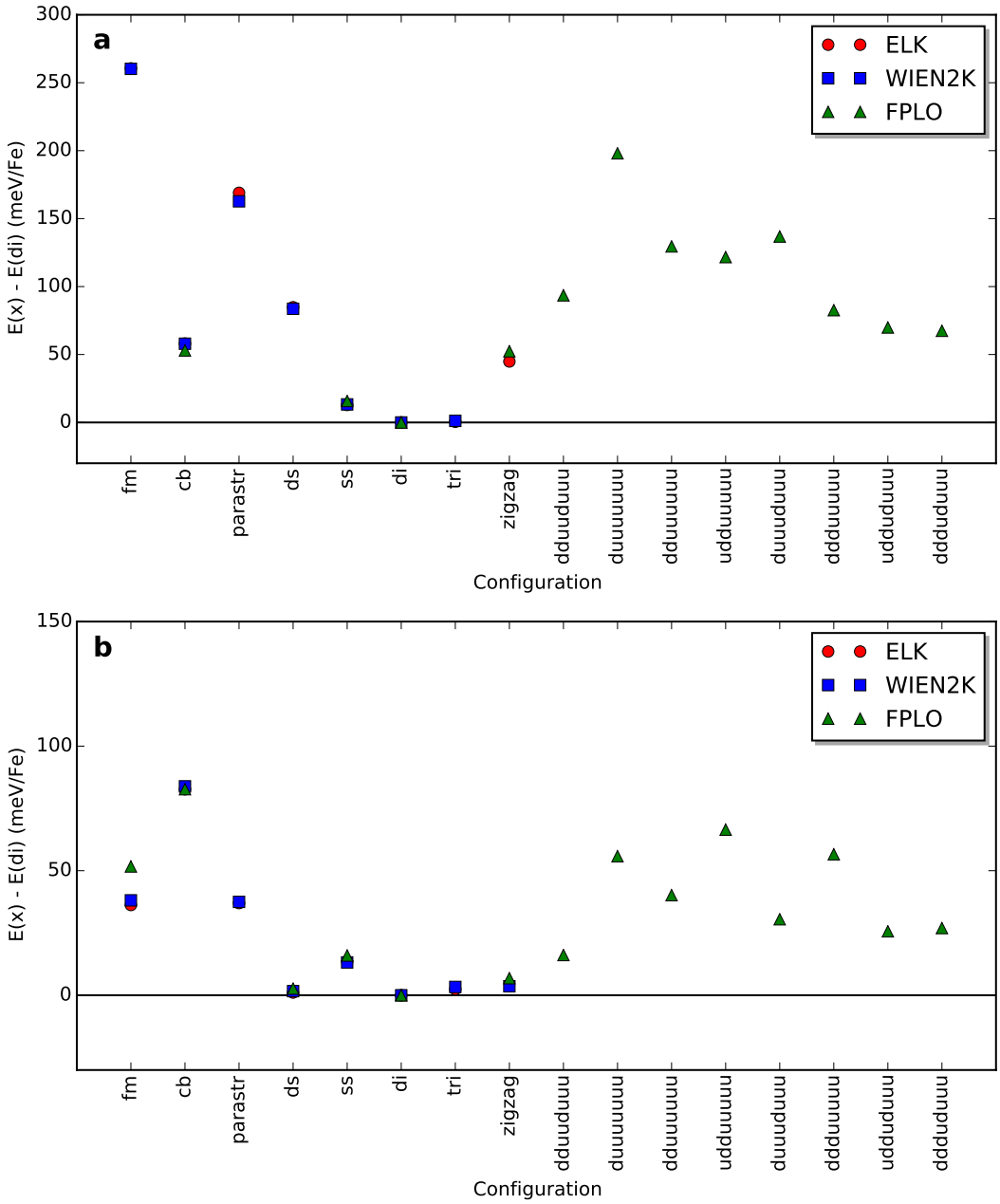

FIG. 6. **Comparison of DFT energies** The DFT energies were calculated using ELK, WIEN2K, and FPLO. **a**, FeSe. **b**, FeTe. See Fig. 5 for the different structures.

Configuration	J_1	J_2	J_3	Const.
Checkerboard	-2	2	2	1
Single Stripes	0	-2	2	1
Double Stripes	0	0	-2	1
Dimers	-1	0	0	1
Trimers	-2/3	-2/3	2/3	1

TABLE III. **The J_1, J_2, and J_3 coefficients.** The coefficients obtained by summing over neighbors of the magnetic structures used for fitting to the J_1-J_2-J_3-K model.

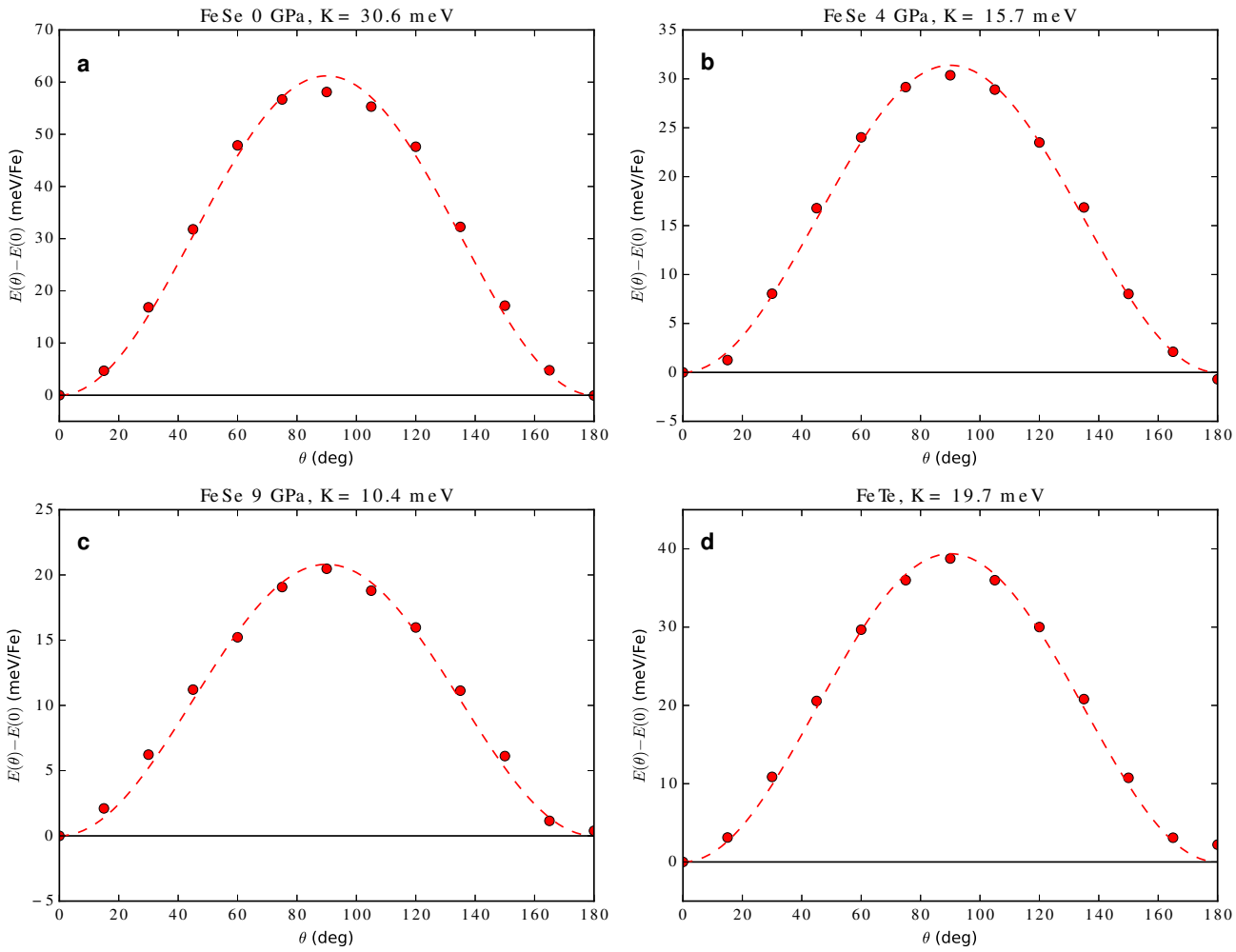

FIG. 7. **Energies of noncollinear structures for FeSe and FeTe as a function of the rotation angle.** The dashed lines are the model fits. **a**, FeSe at 0 GPa pressure. **b**, FeSe at 4 GPa pressure. **c**, FeSe at 9 GPa pressure. **d**, FeTe.

Phase boundary	Ising	Heisenberg	J_1-J_2-J_3-K
cb/di	$2J_3 + 2J_2 - J_1$		$2J_3 + 2J_2 - J_1$
cb/ss			
ss/di	$2J_3 - 2J_2 + J_1$		$4J_3 - 2J_2 + J_1 - 2K$
di/ds	$2J_3 - J_1$		$2J_3 - J_1$
cb/$\mathbf{q} = (\pi, Q)$		$4J_3 + 2J_2 - J_1$	$4J_3 + 2J_2 - J_1 - 2K$
ss/$\mathbf{q} = (\pi, Q)$		$4J_3 - 2J_2 + J_1$	$4J_3 - 2J_2 + J_1 - 2K$
cb/$\mathbf{q} = (Q, Q)$		$4J_3 + 2J_2 - J_1$	$4J_3 + 2J_2 - J_1 - 2K$
$\mathbf{q} = (\pi, Q)$/$\mathbf{q} = (Q, Q)$		$2J_3 - J_2$	$2J_3 - J_2 - K$
di/$\mathbf{q} = (\pi, Q)$			$4K\,(2J_3 - K) - (2J_2 - J_1)^2$
di/$\mathbf{q} = (Q, Q)$			$(J_1 - J_2 - 4J_3 + 3K)^2 - J_1\,(J_1 + J_2 + K) + 2J_1^2$
ds/$\mathbf{q} = (\pi, Q)$			$8J_3\,(2J_3 - J_1) - (2J_2 - J_2)^2 - (2K - J_1)^2 + J_1^2$
ds/$\mathbf{q} = (Q, Q)$			$8J_3K + 4J_2K - 4K^2 - J_1^2$

TABLE IV. **Analytical solutions for phase boundaries of the Ising, Heisenberg, and J_1-J_2-J_3-K models.**